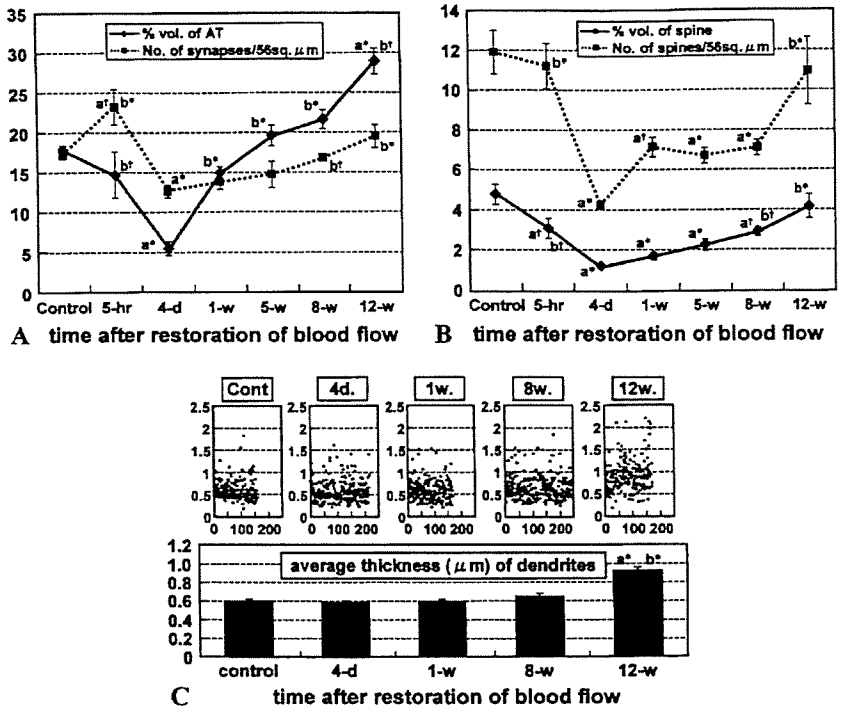

Figure 6. A, Time course of percent volume of axon terminals and number of synapses in the neuropil at various time after ischemic insult. B, Time course of percent volume and number of spines in the neuropil at various time post ischemia. C, Time course by scatter graph (upper) and average thickness (lower) of neurites in the neuropil after the ischemic insult. [a]Compared with control; [b]compared with 4 days; *$P<0.001$, †$P<0.05$.

neurons showed a decreased spine number and segmental dendritic beading after temporary hypoxia/hypoglycemia followed by recovery,[11,12] and a LMS study using horseradish protein injection showed beading of dendrites in the CA-1 of the hippocampus after temporary ischemia.[14] Also an EM study on the CA-1 showed degeneration and shrinkage of dendrite around 3 to 4 days after temporary ischemia.[15–17] In the present study, we found that the neurites degenerated around 4 days and that their thickness increased, in association with the recovery to normal of the number and percent volume of spines, at 12 weeks after the insult.

From 1 to 12 weeks after the ischemic insult, we found that the synaptic number increased gradually in association with an increase in the volume of axon terminals showing sprouting. The present study also showed an increase in the number of the MSBs from 8 to 12 weeks after the ischemic insult, which increase was associated with one in the number and volume of axon terminals and spines. The MSBs represent 2 independent dendritic spines contacting the same axon terminal.[23] One spine branched to make synapses at >2 portions of 1 axon terminal is considered to facilitate neurotransmission.[10] In another study, there was an increase in the number of MSBs in CA-1, paralleling the marked increase in the number of synaptic vesicles after temporary ischemia[7] and after temporary hypoxia/hypoglycemia in hippocampal slices.[10]

From 4 days to 12 weeks after the ischemic insult, some axons attached to the dying neurons showed an abnormal distension of their terminals, which contained degenerated mitochondria, laminated dense bodies, and irregularly located neurofilaments and microtubules (degenerated axon).[8,9] They were frequently observed around accumulations of the electron-dense granular fragments of the dead neurons.

Some axon terminals encrusted with the electron-dense granular fragments of the dead neurons became connected to the spines and neurites of the surviving neurons. These axon terminals, previously attached to the dying and/or dead neurons, seemed to become newly connected to the spines and to the thickened dendrites of the surviving neurons associated with synaptogenesis in the neuropil.[24] However, it could also be that some of these axon terminals were originally contacting more than one dendrites or spines.

Clinically, most stroke survivors show recovery from behavioral dysfunctions. The short-term recovery may be attributable to the resolution of brain edema. A more gradual recovery, promoted by exercise for rehabilitation, may be attributed to the anatomical and functional recovery of the penumbra. Stroemer[24] reported behavioral recovery after neocortical infarction in rats, which recovery was associated with neuronal sprouting followed by synapto-genesis, as demonstrated by immunohistochemical staining for GAP-43, a growth-associated protein expressed on axonal growth cones, and for synaptophysin. Functional remodeling of the cerebral cortex remote from the infarction was detected by intracortical microstimulation mapping of the hand of the squirrel monkey.[25,26]

Activation of the complement system was shown to promote neuronal survival and tissue remodeling.[27] Postischemic treatment with brain-derived neurotrophic factor and physically exercised animals had better functional motor recovery, attributable to induction of widespread neuronal remodeling, as demonstrated by MAP1B and synaptophysin expression.[19] Clinical introduction of novel agents and functional methods to promote synaptogenesis and neuronal networks in the iscehmic penumbra, is highly anticipated.

Summary

In the penumbra around a focal infarction of the cerebral cortex, synapses, synaptic vesicles, axon terminals, spines

degenerated, with a reduction in their number and size, until 4 days and then recovered from 1 to 12 weeks after the ischemic insult.

Source of Funding

This work was supported in part by grant from the Japanese Ministry of Health, Labor and Welfare, Research on Psychiatric and Neurological Diseases (H16-kokoro-017 to K.O.)

References

1. Hanyu S, Ito U, Hakamata Y, Nakano I. Topographical analysis of cortical neuronal loss associated with disseminated selective neuronal necrosis and infarction after repeated ischemia. *Brain Res.* 1997;767:154–157.
2. Ito U, Hanyu S, Hakamata Y, Kuroiwa T, Yoshida M. Features and threshold of infarct development in ischemic maturation phenomenon. In: Ito U, Kirino T, Kuroiwa T, Klatzo I 2nd, eds. *Maturation Phenomenon in Cerebral Ischemia.* Berlin, Heidelberg: Springer-Verlag; 1997:115–121.
3. Luscher C, Nicoll RA, Malenka RC, Muller D. Synaptic plasticity and dynamic modulation of the postsynaptic membrane. *Nat Neurosci.* 2000; 3:545–550.
4. von Lubitz DK, Diemer NH. Cerebral ischemia in the rat: ultrastructural and morphometric analysis of synapses in stratum radiatum of the hippocampal CA-1 region. *Acta Neuropathol (Berl).* 1983;61:52–60.
5. Martone ME, Jones YZ, Young SJ, Ellisman MH, Zivin JA, Hu BR. Modification of postsynaptic densities after transient cerebral ischemia: a quantitative and three-dimensional ultrastructural study. *J Neurosci.* 1999;19:1988–1997.
6. Liu CL, Martone ME, Hu BR. Protein ubiquitination in postsynaptic densities after transient cerebral ischemia. *J Cereb Blood Flow Metab.* 2004;24:1219–1225.
7. Briones TL, Suh E, Jozsa L, Hattar H, Chai J, Wadowska M. Behaviorally-induced ultrastructural plasticity in the hippocampal region after cerebral ischemia. *Brain Res.* 2004;997:137–146.
8. Crain BJ, Evenson DA, Polsky K, Nadler JV. Electron microscopic study of the gerbil dentate gyrus after transient forebrain ischemia. *Acta Neuropathol (Berl).* 1990;79:409–417.
9. Ishimaru H, Casamenti F, Ueda K, Maruyama Y, Pepeu G. Changes in presynaptic proteins, SNAP-25 and synaptophysin, in the hippocampal CA1 area in ischemic gerbils. *Brain Res.* 2001;903:94–101.
10. Jourdain P, Nikonenko I, Alberi S, Muller D. Remodeling of hippocampal synaptic networks by a brief anoxia-hypoglycemia. *J Neurosci.* 2002;22: 3108–3116.
11. Park JS, Bateman MC, Goldberg MP. Rapid alterations in dendrite morphology during sublethal hypoxia or glutamate receptor activation. *Neurobiol Dis.* 1996;3:215–227.
12. Hasbani MJ, Schlief ML, Fisher DA, Goldberg MP. Dendritic spines lost during glutamate receptor activation reemerge at original sites of synaptic contact. *J Neurosci.* 2001;21:2393–2403.
13. Akulinin VA, Stepanov SS, Semchenko VV, Belichenko PV. Dendritic changes of the pyramidal neurons in layer V of sensory-motor cortex of the rat brain during the postresuscitation period. *Resuscitation.* 1997;35: 157–164.
14. Hori N, Carpenter DO. Functional and morphological changes induced by transient in vivo ischemia. *Exp Neurol.* 1994;129:279–289.
15. Petito CK, Pulsinelli WA. Delayed neuronal recovery and neuronal death in rat hippocampus following severe cerebral ischemia: possible relationship to abnormalities in neuronal processes. *J Cereb Blood Flow Metab.* 1984;4:194–205.
16. Yamamoto K, Hayakawa T, Mogami H, Akai F, Yanagihara T. Ultrastructural investigation of the CA1 region of the hippocampus after transient cerebral ischemia in gerbils. *Acta Neuropathol (Berl).* 1990;80: 487–492.
17. Tomimoto H, Yanagihara T. Golgi electron microscopic study of the cerebral cortex after transient cerebral ischemia and reperfusion in the gerbil. *Neuroscience.* 1994;63:957–967.
18. Graham DI, Lantos PL. In: Greenfield's Neuropathology, 7th ed. Arnold, London; 2002:233–355.
19. Schabitz WR, Berger C, Kollmar R, Seitz M, Tanay E, Kiessling M, Schwab S, Sommer C. Effect of brain-derived neurotrophic factor treatment and forced arm use on functional motor recovery after small cortical ischemia. *Stroke.* 2004;35:992–997.
20. Ito U, Spatz M, Walker J Jr, Klatzo I. Experimental cerebral ischemia in mongolian gerbils. I. Light microscopic observations. *Acta Neuropathol Berl.* 1975;32:209–223.
21. Ohno K, Ito U, Inaba Y. Regional cerebral blood flow and stroke index after left carotid artery ligation in the conscious gerbil. *Brain Res.* 1984; 297:151–157.
22. Weibel ER. Morphometry of the human lung. Springeer-Verlag, Berlin, Gowttingen, Heidelberg; 1963:19–22.
23. Sorra KE, Harris KM. Occurrence and three-dimensional structure of multiple synapses between individual radiatum axons and their target pyramidal cells in hippocampal area CA1. *J Neurosci.* 1993;13: 3736–3748.
24. Stroemer RP, Kent TA, Hulsebosch CE. Neocortical neural sprouting, synaptogenesis, and behavioral recovery after neocortical infarction in rats. *Stroke.* 1995;26:2135–2144.
25. Frost SB, Barbay S, Friel KM, Plautz EJ, Nudo RJ. Reorganization of remote cortical regions after ischemic brain injury: a potential substrate for stroke recovery. *J Neurophysiol.* 2003;89:3205–3214.
26. Nudo RJ, Larson D, Plautz EJ, Friel KM, Barbay S, Frost SB. A squirrel monkey model of poststroke motor recovery. *Ilar J.* 2003;44:161–174.
27. van Beek J, Elward K, Gasque P. Activation of complement in the central nervous system: roles in neurodegeneration and neuroprotection. *Ann N Y Acad Sci.* 2003;992:56–71.

Acta Neurochir (2006) [Suppl] 96: 239–243

Printed in Austria

Restitution of ischemic injuries in penumbra of cerebral cortex after temporary ischemia

U. Ito[1,3], E. Kawakami[1], J. Nagasao[1], T. Kuroiwa[2], I. Nakano[3], and K. Oyanagi[1]

[1] Department of Neuropathology, Tokyo Metropolitan Institute for Neuroscience, Tokyo, Japan
[2] Department of Neuropathology, Medical Research Institute, Tokyo Medical and Dental University, Tokyo, Japan
[3] Department of Neurology, Jichi Medical School, Tochigi, Japan

Summary

We investigated, at both light and ultrastructural levels, the fate of swollen astrocytes and remodeling of neurites connected to disseminated, dying neurons in the ischemic neocortical penumbra. Specimens from left cerebral cortex were cut coronally at the infundibulum and observed by light and electron microscopy. We measured synapses and spines, and the thickness of neuritic trunks in the neuropil on electron microscopy photos. We also determined percent volume of axon terminals and spines by Weibel's point-counting method. Astrocytic swelling gradually subsided from day 4 after the ischemic insult, with increases in cytoplasmic glial fibrils and GFAP-positive astrocytes. Disseminated dying electron-dense neurons were fragmented by invading astrocytic cell processes and accumulated as granular pieces. The number of synapses and spines and total percent volume of axon terminals and spines decreased with an increasing sparsity of synaptic vesicles until day 4. One to 12 weeks after the ischemic insult, these values increased to or exceeded control values, and sprouting and increased synaptic vesicles were seen. Axons that had been attached to the dying neurons appeared to have shifted their connections to the spines and the neurites of the surviving neurons, increasing their thickness. Astrocytic restitution and neuronal remodeling processes started at 4 days continuing until 12 weeks after ischemic insult.

Keywords: Maturation phenomenon; cerebral ischemia; neuronal remodeling.

Introduction

Cerebral infarction develops rapidly after a major ischemic insult. Earlier, we developed a model to induce an ischemic penumbra around a small focal infarction in the cerebral cortex of Mongolian gerbils [5, 8] by giving a threshold amount of ischemic insult to induce cerebral infarction. The histopathology of this model revealed disseminated eosinophilic ischemic neurons by light microscopic observation, and disseminated electron-dense neurons seen ultrastructurally (disseminated selective neuronal necrosis) increased in number in the penumbra of the cerebral cortex after restoration of blood flow. A focal infarction developed later in a part of this area of disseminated selective neuronal necrosis within 12 to 24 hours after ischemic insult, due to massive astrocytic death. This area expanded gradually, involving dead and still-living eosinophilic neurons, and normal-looking neurons progressing to death 4 days after the ischemic insult [8, 9, 11]. No additional new infarction (pan necrosis) was found later than 4 days after the ischemic insult in our coronal as well as para-sagittal sections of the forebrain [3, 19].

In previous studies of the cortical penumbra [7, 9, 11], we found that the cytoplasm and cell processes of living astrocytes in the penumbra were actively swollen and that brain edema, determined by tissue gravimetry, was maximum around 3 days after ischemic insult, subsiding gradually by 7 days [4, 11]. Isolated dark neurons with different grades of high-electron density increased in number among the normal-looking neurons from 5 to 24 hours. These dark neurons were surrounded by severely swollen astrocytic cell processes. As a general pathological sign of irreversible cellular damage, granular chromatin condensation was apparent in the nuclear matrix and along the nuclear membrane of some of these dark neurons [12]. The dark neurons increased in number rapidly until day 4, and new ones continued to appear 12 weeks after the ischemic insult. These observations correspond to the maturation phenomenon of ischemic injuries [3, 6, 19], which is the same as the delayed neuronal death described for CA1 neurons [3, 15, 19].

In the present study, we investigated the fate of swollen edematous astrocytes and dead neurons at the ultrastructural level, as well as remodeling of axons connected to the dead neurons in the ischemic penumbra.

Materials and methods

Stroke-positive Mongolian gerbils were selected according to their stroke index score [18] during left carotid clipping for 10 minutes, followed by another 10 minutes of clipping with a 5-hour interval between the 2 occlusions. The gerbils were sacrificed at 5, 12, and 24 hours, at 4 days, and at 3, 5, 8, 12, and 24 weeks following the last ischemic insult by intracardiac perfusion with cacodylate-buffered glutaraldehyde fixative (3 animals in each group) for electron microscopy and with 10% phosphate-buffered formaldehyde fixative for light microscopy (5 animals in each group).

Ultrathin sections including the second through fifth cortical layers were obtained from the neocortex at the mid-point between the interhemispheric and rhinal fissures on the left coronal face sectioned at the infundibular level, in which only the penumbra appeared. The sections were double-stained with uranyl acetate and lead solution, and observed with a Hitachi electron microscope (H9000). Separate paraffin sections were stained with hematoxylin-eosin, periodic acid fuchsin Schiff, or by Bodian silver impregnation or immuno-histochemistry for glial fibrillary acidic protein (GFAP).

Placing 1 cm × 1 cm lattices on the 5,000 × 2.67 enlarged EM photographs, we measured the number of synapses and spines in the neuropil in a 100-square cm (56 sq.μ, by real size), and determined the percent volume of the axon terminals and spines using the point-counting method [22] by counting intersections of the lattice dropped on the axon terminals and/or spines. We also measured neuritic thickness as the maximal diameter perpendicular to their neurofilaments and/or microtubules on the same EM pictures.

Results

Astrocytic swelling gradually subsided starting on day 4 after ischemic insult, then an increase was observed in the number of cytoplasmic glial fibrils in astrocytes seen ultrastructurally and in GFAP-positive cells seen by light microscopy. Astrocytes in mitosis or with 2 nuclei were occasionally seen.

The disseminated dying electron-dense neurons had been fragmented into granular pieces by invading astrocytic cell processes (Fig. 1A). These accumulations of fragmented dark neurons were observed as eosinophilic ghost cells by light microscopy. The electron-dense granular pieces were dispersed around the extracellular spaces and phagocytized by microglia, astrocytes, and neurons. There was no evidence of macrophages in the penumbra.

The number of synapses and spines, and the percent volume of the axon terminals and spines (Table 1) decreased with an increase in a sparsity of synaptic vesicles until day 4 (Fig. 2A). From 1 to 12 weeks after ischemic insult, however, they recovered to or exceeded the control values and were found surrounding the thickened neurites of the surviving neurons (Fig. 2B).

From 4 days to 8 weeks after the ischemic insult, most axon terminals that had been attached to dying neurons were found around the fragmented dead dark neurons. Some of them were separated from the dead neurons, being attached by a crust of granular electron-dense fragments (Fig. 1A). From 24 hours to 8 weeks after ischemic insult, some axons attached to dying neurons showed globular or spindle-shaped distension of their terminals, as seen by Bodian silver impregnation (Fig. 1B). Electron microscopic observation of these distensions showed amplified axon terminals containing degenerated mitochondria, lamellated dense bodies, and irregularly located neurofilaments and microtubules. They were frequently observed around accumulations of fragmented electron-dense granular pieces of dead neurons.

From 1 to 12 weeks, some axon terminals associated with crusts of electron-dense granular pieces became newly connected to the spines and neurites of the surviving neurons.

Neuronal death continued in the penumbra during these periods (maturation phenomenon). From 8 to 24 weeks after the ischemic insult, these structures and the accumulation of eosinophilic ghost cells remained confined to the third cortical layer, especially in some portions of the lateral part of the left coronal face sectioned at the infundibular level. Cortical thickness and cortical neuronal density were reduced evenly in the face during these periods.

Discussion

Astrocytes swell in the acute phase after an ischemic insult, showing increases in the number of glycogen granules and mitochondrial size and number, indicating an active reaction of astrocytes to prevent ischemic neuronal injury [7, 11]. Four days after ischemic insult, astrocytic swelling subsides and glial fibrils, stained by GFAP antibodies, increase in number. These GFAP-positive reactive astrocytes are increased in number by mitotic division, especially those surrounding the focal infarction (pan necrosis), which evolves and develops from 12 hours to 4 days after the insult. Necrotic tissue is then scavenged by macrophages and

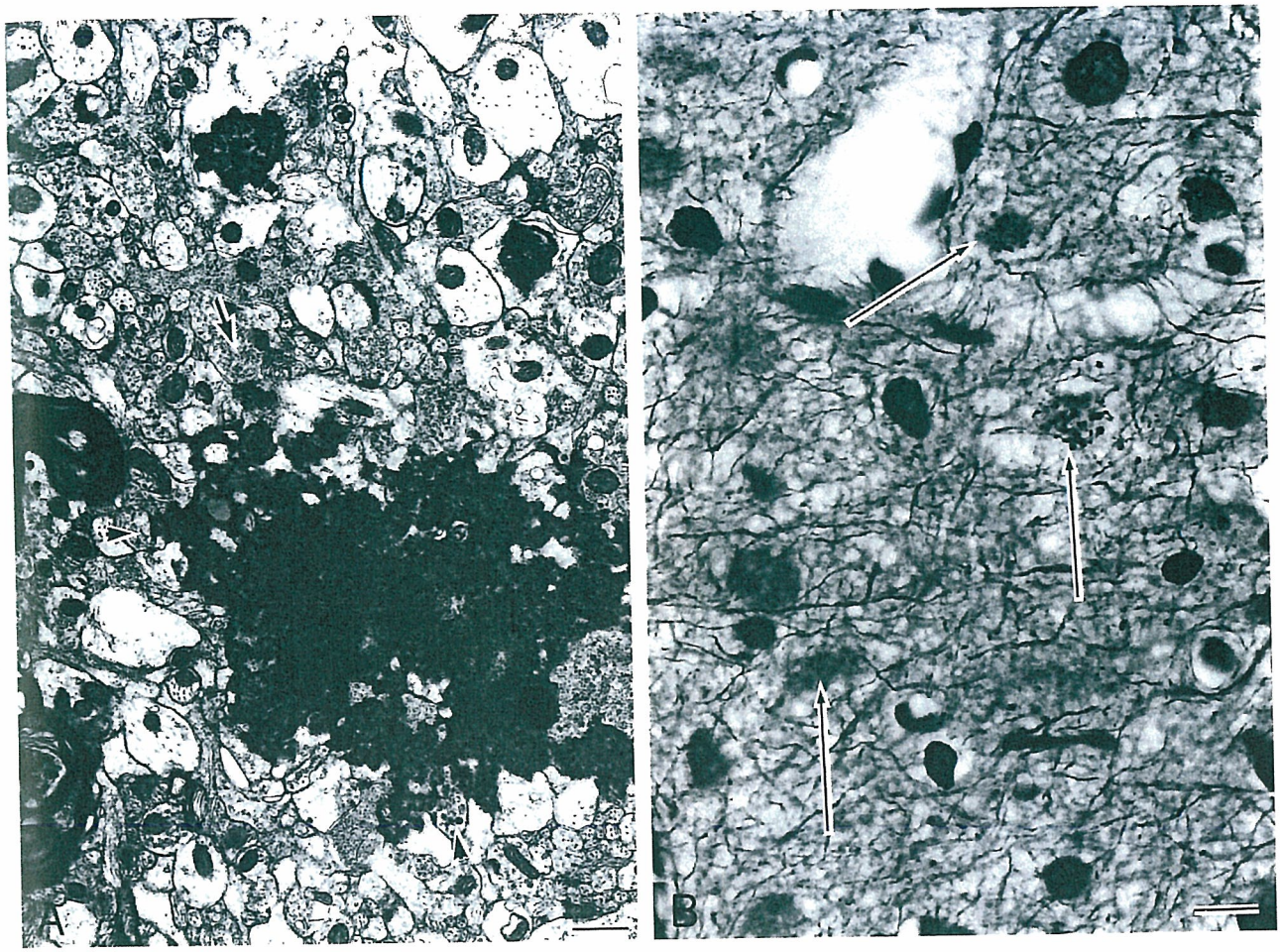

Fig. 1. (A) Electron microscopy of cerebral cortex 4-days after restoration of blood flow. The disseminated dying electron-dense neuron has been fragmented into granular pieces by invading astrocytic cell processes. Some axon terminals that were attached to the dying neurons are found around the fragmented dead dark neurons (arrowheads). Bottom bar 0.1 micron. (B) Light microscopy of cerebral cortex 24 hours after restoration of blood flow. Some thick axons attached to dying neurons showed globular or spindle-shaped distension of their terminals surrounding the dead neurons (arrows). Bodian silver impregnation. Bottom bar 2 micron

Table 1. *Data showing astrocytic restitution and neuronal remodeling processes up to 12 weeks after ischemic injury.*

Average value	Time after last ischemic insult						
	Control	5 hours	4 days	1 week	5 weeks	8 weeks	12 weeks
% vol. of axon terminal	17.75 ± 1.32	14.69 ± 5.79†	5.48 ± 1.71*	14.89 ± 1.69†	19.55 ± 2.62†	21.62 ± 2.24†	28.90 ± 3.55*†
% vol. of spine	4.80 ± 1.12	3.09 ± 0.89*†	1.19 ± 0.20*	1.70 ± 0.25*	2.25 ± 0.45*	2.91 ± 0.42*†	4.16 ± 1.04†
No. of synapses/56 sq μ	17.21 ± 1.09	23.24 ± 4.52*†	12.65 ± 1.67*	13.80 ± 1.92†	14.71 ± 3.26	16.68 ± 1.55†	19.48 ± 3.10†
No. of spines/56 sq μ	11.89 ± 2.50	11.20 ± 2.33†	4.26 ± 0.40*	7.14 ± 0.78*	6.69 ± 0.63*	7.10 ± 0.68*	10.93 ± 3.04†
Thickness of neuritis (μ)	0.61 ± 0.02	–	0.59 ± 0.02	0.60 ± 0.02	–	0.67 ± 0.02*†	0.93 ± 0.03*†

Average ± standard error, $p < 0.05$: * compared with control; † compared with 4 days.

becomes liquefied [3, 8, 19]. The infarcted focus is surrounded by gliosis induced by reactive astrocytes. GFAP-positive reactive astrocytes increase moderately in number, but do not induce gliosis in the penumbra. These are the restitutional processes of astrocytes in the ischemic tissue [8].

It has been thought that dead neurons and ischemically injured tissue are scavenged by macrophage inva-

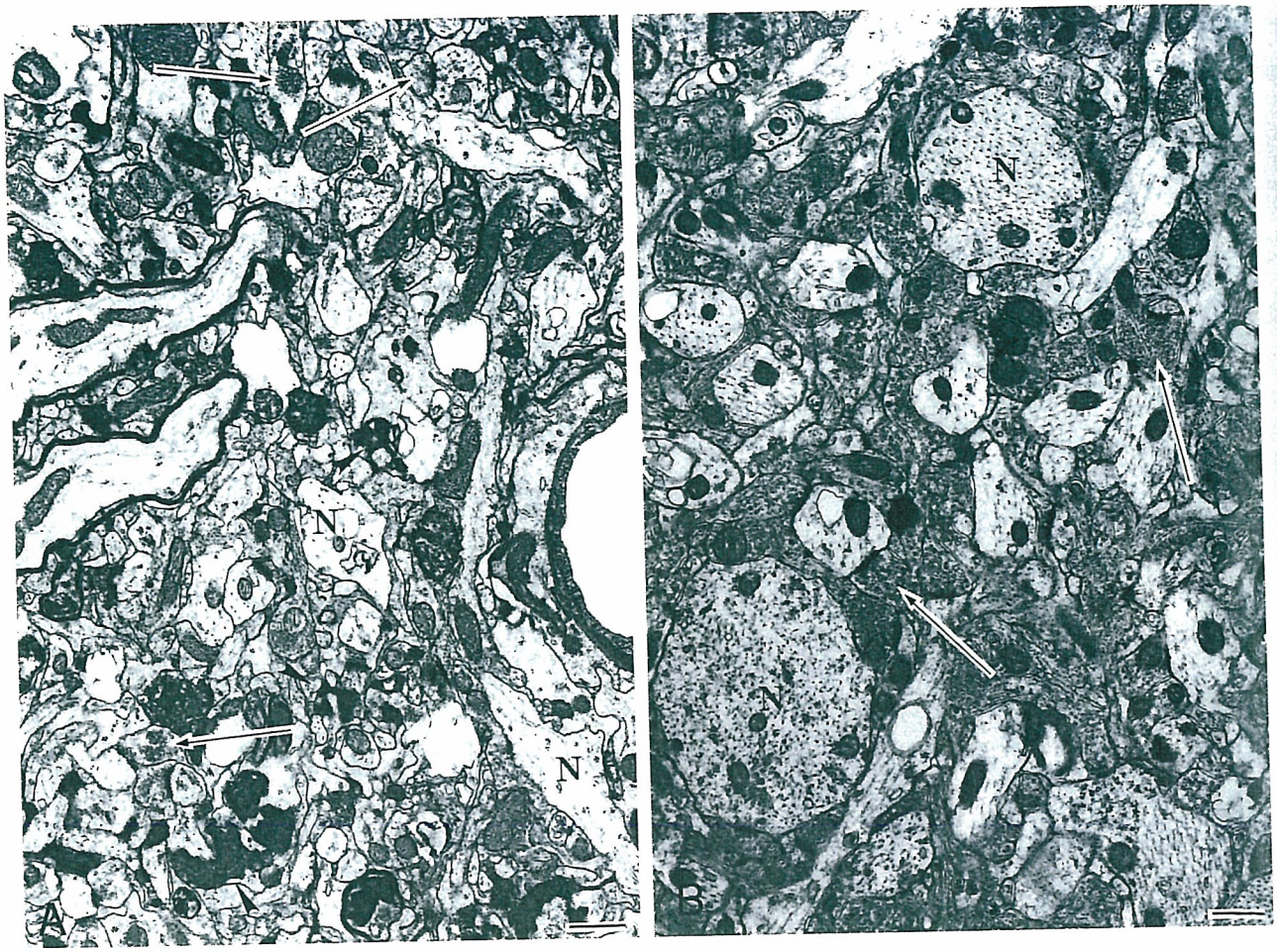

Fig. 2. (A) Electron microscopy of cerebral cortex 4 days after restoration of blood flow. The number of synapses and spines, and the volume of axon terminals and spines decreased with increase in sparsity of synaptic vesicles (arrows). Neurites (*N*) are degenerative. Electron-dense granular pieces are dispersed in the extracellular spaces of the neuropil (arrowheads). Bottom bar 0.1 micron. (B) Electron microscopy of cerebral cortex 12 weeks after restoration of blood flow. The number of synapses and spines, and volume of axon terminals and spines recovered, with increase in number of synaptic vesicles (arrows). Neurites (*N*) are thickened, surrounded and/or synapsed by axon terminals. Bottom bar 0.1 micron

sion into the injured tissue from the blood stream. However, in the present study, dead neurons were found disseminated among surviving neurons in the cortical penumbra. The axons and dendritic processes of the dying neurons were still connected to axon terminals and neurites of surviving neurons. Solitary dying neurons, which were connected by neuritic networks, were not phagocytized by a single macrophage. In contrast to infarction, i.e., massive necrosis, macrophages did not enter the neuropil of the penumbra where the network of the neuropil was still tight. In this situation, it is reasonable to assume that shrunken dead neurons become fragmented into granular debris (eosinophilic ghost cells seen by the light microscopy) and are removed by astrocytes, neurons, and perivascularly located microglia [10, 14, 16]. However, the tattered central cytosol of shrunken neurons remained for more than 5 weeks. No inflammatory cells or macrophages appeared in the ischemic penumbra wandering in the neuropils [10, 16].

We found a marked decrease in the number of synapses and volume of the axon terminals in the entire neuropil of the ischemic penumbra from 5 hours to 4 days after start of recirculation, along with marked shrinkage of axon terminals, which contained a decreased number of synaptic vesicles. These changes seemed to be due to calcium-dependent neuronal hyperexcitation [21] and were reduced by N-methyl-D-aspartate receptor antagonists in a morphological study recording excitatory postsynaptic potential

from hippocampal slice cultures subjected to brief anoxia-hypoglycemia [13].

The number of synapses increased gradually from 1 to 12 weeks after the ischemic insult, associated with an increase in the volume of axon terminals showing sprouting [20] and paralleling a marked increase in the number of synaptic vesicles. The number and volume of spines also increased in parallel. Axons that had been attached to the dying neurons were considered to have shifted their connections to the spines and the neurites of the surviving neurons, increasing their thickness associated with synaptogenesis in the neuropil [1, 2, 17]. The neuronal remodeling process progressed in the ischemic penumbra from its early stage to 12 weeks after the start of recirculation.

References

1. Crepel V, Epsztein J, Ben-Ari Y (2003) Ischemia induces short- and long-term remodeling of synaptic activity in the hippocampus. J Cell Mol Med 7: 401–407
2. Frost SB, Barbay S, Friel KM, Plautz EJ, Nudo RJ (2003) Reorganization of remote cortical regions after ischemic brain injury: a potential substrate for stroke recovery. J Neurophysiol 89: 3205–3214
3. Graham DI, Lantos PL (2002) Greenfield's neuropathology illustrated. Oxford University Press, London, pp 230–280
4. Hakamata Y, Hanyu S, Kuroiwa T, Ito U (1997) Brain edema associated with progressive selective neuronal death or impending infarction in the cerebral cortex. Acta Neurochir [Suppl] 70: 20–22
5. Hanyu S, Ito U, Hakamata Y, Nakano I (1997) Topographical analysis of cortical neuronal loss associated with disseminated selective neuronal necrosis and infarction after repeated ischemia. Brain Res 767: 154–157
6. Ito U, Spatz M, Walker JT Jr, Klatzo I (1975) Experimental cerebral ischemia in mongolian gerbils. I. Light microscopic observations. Acta Neuropathol Berl 32: 209–223
7. Ito U, Hanyu S, Hakamata Y, Nakamura M, Arima K (1997) Ultrastructure of astrocytes associated with selective neuronal death of cerebral cortex after repeated ischemia. Acta Neurochir [Suppl] 70: 46–49
8. Ito U, Hanyu S, Hakamata Y, Arima K, Oyanagi K, Kuroiwa T, Nakano I (1999) Temporal profile of cortical injury following ischemic insult just-below and at the threshold level for induction of infarction – light and electron microscopic study. In: Ito U, Fieschi C, Orzi F, Kuroiwa T, Klatzo I (eds) Maturation phenomenon in cerebral ischemia III. Springer, Berlin New York, pp 227–235
9. Ito U, Kuroiwa T, Hanyu S, Hakamata Y, Nakano I, Oyanagi K (2000) Ultrastructural behavior of astrocytes to singly dying cortical neurons. In: Krieglstein J, Klumpp S (eds) Pharmacology of cerebral ischemia. Medpharm Science Publications, Stuttgart, pp 285–291
10. Ito U, Kuroiwa T, Hakamata Y, Kawakami E, Nakano I, Oyana K (2002) How are ischemically dying eosinophilic neurons scavenged in the penumbra? An ultrastructural study. In: Krieglstein J, Klumpp S (eds) Pharmacology of cerebral ischemia. Medpharm Science Publication, Stuttgart, pp 261–265
11. Ito U, Kuroiwa T, Hanyu S, Hakamata Y, Kawakami E, Nakano I, Oyanagi K (2003) Temporal profile of experimental ischemic edema after threshold amount of insult to induce infarction – ultrastructure, gravimetry and Evans' blue extravasation. Acta Neurochir [Suppl] 86: 131–135
12. Ito U, Kuroiwa T, Hanyu S, Hakamata Y, Kawakami E, Nakano I, Oyanagi K (2003) Ultrastructural temporal profile of the dying neuron and surrounding astrocytes in the ischemic penumbra: apoptosis or necrosis? In: Buchan AM, Ito U, Colbourne F, Kuroiwa T, Klatzo I (eds) Maturation phenomenon in cerebral ischemia V. Springer, Berlin Heidelberg, pp 189–196
13. Jourdain P, Nikonenko I, Alberi S, Muller D (2002) Remodeling of hippocampal synaptic networks by a brief anoxia-hypoglycemia. J Neurosci 22: 3108–3116
14. Kalmar B, Kittel A, Lemmens R, Kornyei Z, Madarasz E (2001) Cultured astrocytes react to LPS with increased cyclooxygenase activity and phagocytosis. Neurochem Int 38: 453–461
15. Kirino T, Tamura A, Sano K (1984) Delayed neuronal death in the rat hippocampus following transient forebrain ischemia. Acta Neuropathol Berl 64: 139–147
16. Lemkey-Johnston N, Butler V, Reynolds WA (1976) Glial changes in the progress of a chemical lesion. An electron microscopic study. J Comp Neurol 167: 481–501
17. Nudo RJ, Larson D, Plautz EJ, Friel KM, Barbay S, Frost SB (2003) A squirrel monkey model of poststroke motor recovery. ILAR J 44: 161–174
18. Ohno K, Ito U, Inaba Y (1984) Regional cerebral blood flow and stroke index after left carotid artery ligation in the conscious gerbil. Brain Res 297: 151–157
19. Rosenblum WI (1997) Histopathologic clues to the pathways of neuronal death following ischemia/hypoxia. J Neurotrauma 14: 313–326
20. Stroemer RP, Kent TA, Hulsebosch CE (1995) Neocortical neural sprouting, synaptogenesis, and behavioral recovery after neocortical infarction in rats. Stroke 26: 2135–2144
21. von Lubitz DK, Diemer NH (1983) Cerebral ischemia in the rat: ultrastructural and morphometric analysis of synapses in stratum radiatum of the hippocampal CA-1 region. Acta Neuropathol (Berl) 61: 52–60
22. Weibel ER (1963) Morphometry of the human lung. Springer, Berlin, pp 19–20

Correspondence: Umeo Ito, 4-22-24, Zenpukuji, Suginami-ku, Tokyo 167-0041 Japan. e-mail: umeo-ito@nn.iij4u.or.jp

特別講演より

パーキンソン病・パーキンソン痴呆症とマグネシウム

― 世代にまたがる長期欠乏実験 ―

小柳 清光

東京都神経科学総合研究所

運動・感覚システム研究分野長

文月会誌

第2号 2007年1月

Academic Society for the Metropolitan Alumni of Faculty of Medicine, Niigata University

特別講演より

パーキンソン病・パーキンソン痴呆症とマグネシウム
—世代にまたがる長期欠乏実験—

小柳（おやなぎ） 清光
東京都神経科学総合研究所
運動・感覚システム研究分野長
神経病理学
（D51）

はじめに：神経系はミネラルと深い関係を有している。たとえばカルシウム（Ca）やマグネシウム（Mg）はシナプス伝達には不可欠な物質であり、Mgは神経系にも多量に存在する二百種類をこえる酵素の補酵素で、phosphotransferaseやATPaseなどエネルギー代謝、蛋白・核酸合成、細胞周期、細胞骨格・ミトコンドリアの保全、細胞膜への物質結合などに深く関与しているという[1]。

パーキンソン徴候と認知症状を来すパーキンソン痴呆症（PDC）と運動ニューロン疾患である筋萎縮性側索硬化症（ALS）とが、不思議なことに揃って東経140度線上の紀伊半島、グアム島、西ニューギニアに多発していたという。グアム島での発症のピークは1950-60年頃といわれ、わずか30年ほどで急激に減少したことからも主原因は外因と見なされている。これら三地域では土壌も、飲料となる河川水も、低Ca低Mg高アルミニウム（Al）であるという。このためPDCとALSの発症には、低Ca、低Mg、高Alの飲料水を摂取することが原因ではないかと言うミネラル説[1,2,3,4]と、一方ある種のソテツの実に含まれる興奮性神経毒の摂取が原因ではないか、という神経毒説[5]があり、論議が続けられてきた。これらの仮説に基づいた動物実験が世界中で数多く実施されたが、PDCの中核病変である黒質神経細胞脱落、あるいはALSの基幹病変である脳幹、脊髄の運動ニューロン脱落が証明された報告はこれまで見られない。しかしこれらの実験のほとんどが成熟した動物やせいぜい幼年期の動物を用いた実験であった[6,7,8]。私たちは、「仮に飲み水がPDCやALSの原因だとすれば、それらの患者さんは、発症する壮・老年期になってその水を飲み始めたはずがなく、

子供時代もその水を飲んでいたはずであり、また母の体内にいる胎児のころから、胎盤を通してその水を飲んだに違いない。さらに言えば、その未生の患者さんの両親となる男女がその水を飲んでいたはずである。」と考え、実生活の実態にあった実験を行うのであれば、胎児や子供時代、その前の父親、母親の代からの影響も加味する必要があり、「二世代にまたがる」研究が不可欠ではないか、と考えた。実験には出来ればサルなどヒトに近いと言われる動物を使用したかったのだが、これらの動物の寿命は長く、二世代に亘る実験を実施するには少なくとも10年以上の月日が必要で、そのようなことから実験にはラットを使用した。

世代にまたがるMg、Ca欠乏実験：本実験では低Mg、低Ca摂取の影響を調べることを目的とした。欠乏の閾値を知る目的から、標準飼料のおよそ1/2および1/5にMg、Caの含有量を減らした特殊飼料を6種類作成し（表1）、また欠乏によって障害が生じる時期（臨界期）を知る目的から投与は二世代にまたがり、時期をずらして6段階（i～vi群）設定した（図1）。飲み水

Foods	No.	Mineral contents Ca mg/100g	Mg mg/100g	Al mg/100g	Mn mg/100g	Zn mg/100g	Na mg/100g	K mg/100g	P mg/100g	Drinking Water
Standard		892	78	-	3	3	236	497	664	DDW
Low Ca	#1	400	78	-	3	3	236	497	664	DDW
Low Ca	#2	190	78	-	3	3	236	497	664	DDW
Low Mg	#3	892	40	-	3	3	236	497	664	DDW
Low Mg	#4	892	14	-	3	3	236	497	664	DDW
Low Ca-M	#5	400	40	-	3	3	236	497	664	DDW
Low Ca-M	#6	190	14	-	3	3	236	497	664	DDW

Mineral intake was controled by foods.

表1　飼料（#1～#6）のミネラル含有量。飲み水はDDW（ミリQ水）で、ミネラル摂取は飼料によってコントロールした。

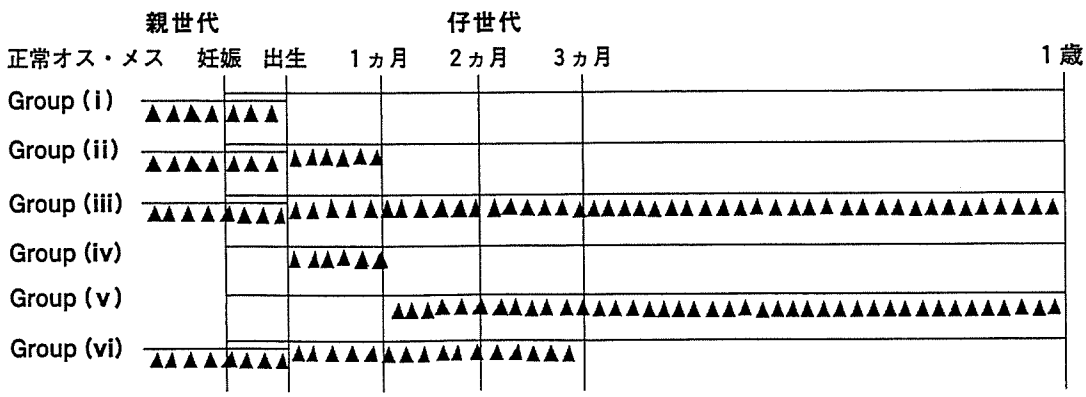

図1　特殊飼料（#1～#6）それぞれの曝露時期を変え（i群～vi群）、ラットに障害が起きる危険な時期（臨界期：critical period）を知る。

は脱イオン蒸留ミリQ水で、飼料によって摂取ミネラルの量を調節した。ウイスターラットを使用し、実験群はオス、メス分けて総数60群、計870匹である。妊娠16日、生後1日、生後1カ月、6カ月、1年で、母または仔から採血して血清中の金属分析を行い、剖検材料を病理学的に検索した。

血中ミネラル濃度の変化：Ca含有を1/5程度まで減らし、1年経過しても血中Ca濃度は減少しなかった。このことは、Caプールが極めて大きいことを示すとともに、排泄量のコントロールが容易であること、血中Ca濃度が生体の維持に不可欠であることを示している。一方Mg含有を1/2まで減らすと血中Mg濃度は2/3に、1/5まで減らすと血中濃度は1/2まで減少した。これは、Mgプールが小さいこと、排泄量をコントロールしにくいこと、また、MgはCaに比べれば、生命の維持という点で重要性が低い、ことを示しているのかもしれない。

体躯と脳の発達：妊娠16日、生後1日には、いずれの実験群でも体重、脳重には正常と差がなく、組織学的にも変化はみられなかった。しかし生後2週以降、Mg欠乏飼料投与群（#4）、Ca-Mg欠乏飼料群（#6）、Ca欠乏飼料群（#2）の順に程度が強い発育障害がみられ、継続的Mg欠乏群（#4、iii）では体重は生後2週から1歳まで、正常のほぼ2/3程度を示した。脳重は、継続的Mg欠乏群（#4、iii）の生後1年では脳重は正常のおよそ90%で、軽度の脳萎縮を呈した（図2）。

また生後1ヵ月で正常餌に切り替えた群（#4、ii）の生後1歳でも脳萎縮が見られた。この事は、胎生期から生後1ヵ月までのMg欠乏が、壮・老年期に脳萎縮を来すことを示している。

黒質のドパミン神経細胞脱落：継続的Mg欠乏群（#4、iii）では、生後6カ月では著変が見られなかったが、1歳で黒質は強

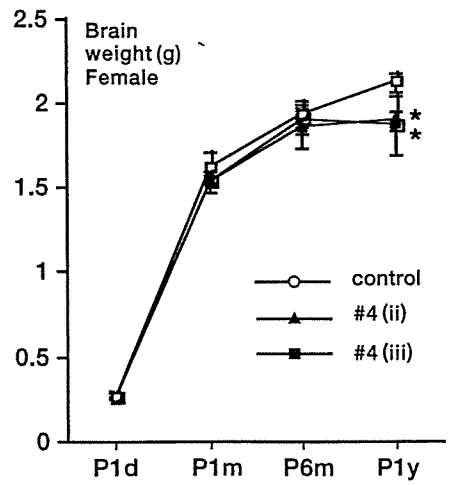

図2 脳重。継続的Mg欠乏ラット（#4，iii群）では、生後6カ月までは脳重には正常との差が無かったが、生後1年、軽度の脳萎縮を示した。生後1ヵ月以降正常餌に戻った群（#4，ii群）でも脳萎縮が見られた。

く萎縮し（図3）、そのドパミン神経細胞の数は正常のほぼ2/3まで減少し、特に神経突起は著明に減少していた（図4）。一方、腹側被蓋野および視床下部のドパミン神経細胞には正常と差がなかった。この群（#4、iii）の1歳のラット黒質の電顕所見では、ミトコンドリア、粗面小胞体、リボゾームの数が少なく、神経細胞核の核膜には深い切れ込みがみられた。また黒質神経細胞では核でタネル染色が陽性であった。これらの所見は飼料中のMgを正常の1/5まで減らした群（#4）、それも妊娠前から生後1年まで継続した群（iii）で最も著明であった。飼料中のCaだけを1/2、1/5まで減

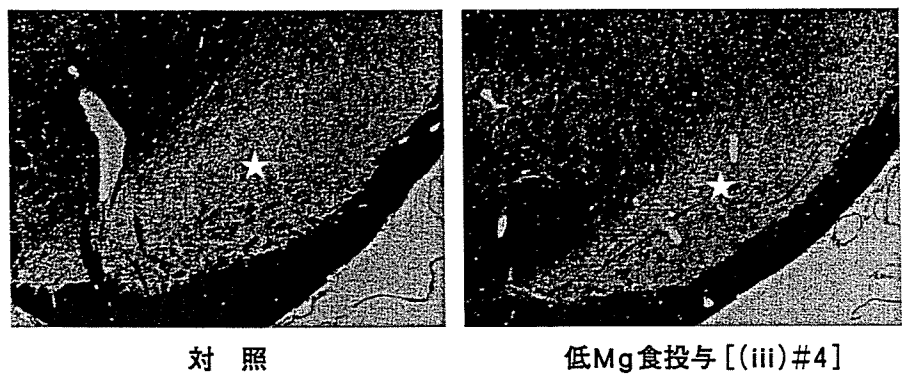

図3　継続的Mg欠乏ラット（#4，iii群）1歳の黒質（★）（b）は、年齢相応の正常対照（a）に比較して強い萎縮を示した。Klüver-Barrera染色。

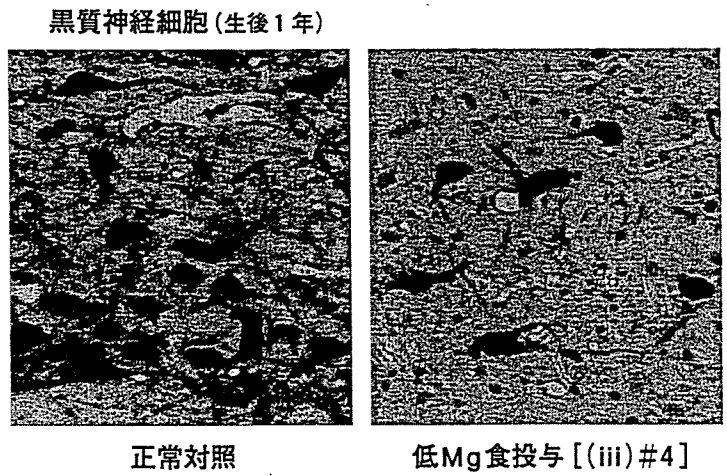

図4　継続的Mg欠乏ラット（#4，iii群）1歳の黒質（b）では、年齢相応の正常対照（a）に比較して、ドパミン神経細胞の数が減少し、特に神経突起の脱落が著明であった。チロシン水酸化酵素免疫染色。

らした群では明らかな変化は認められなかった。いずれの群でも、レビー小体、神経原線維変化、またapoptotic bodyは認められなかった。脊髄には白質、灰白質ともに明らかな変化は認められなかった。

本実験結果は、妊娠前から生後の壮年期まで、Mg欠乏（正常量の1/5）が続くとラットの黒質に選択的なドパミン神経細胞脱落を来すことを示している。その機序は、黒質ドパミン神経細胞の核DNA障害による遺伝情報の障害と、ミトコンドリア、粗面小胞体やリボゾームの障害が重なり合うことによって、細胞内のエネルギー生産系と蛋白合成系を阻害し、神経細胞脱落を惹起するもの、と思われた（図5）。

本実験はグアム島のPDC、ALSを念頭に置いた実験であったが、黒質に神経細胞脱落がみられた一方脊髄には著変なく、この点からもグアム島のALSは、PDCとは原因を異にする疾患である、と考えたい[9]。また黒質の所見はパーキンソン病のそれとも良く類似していた。すなわち本実験結果は、現在原因不明であるヒトのパーキンソン病やパーキンソン痴呆症が、子どもを作る前の父母のMg摂取不足に始まり、妊娠中の母親のMg欠乏、生後患者自身の長期のMg不足が続くことが原因となって発症する可能性があることを世界でも初めて実験的に示した。

日本の社会現象としてのミネラル摂取不足：経口のミネラル欠乏は土地の風土や社会現象などとの関連が深い。上記したグアム島やニューギニアでは風土そのものであった。ところが文明が発達したと思われる現代の日本でも若い世代ほどミネラルの摂取量が少なく、Mgなどは理想の摂取量の半分以下という。過度のダイエットや食生活の変化、特に食事がわりにお菓子を食することなどが原因と言われている。前記した私どもの実験ではMgを正常の1/5まで減らしたラットの仔が、壮年までその餌を食べ続けたとき黒質変性を生じた。一世代

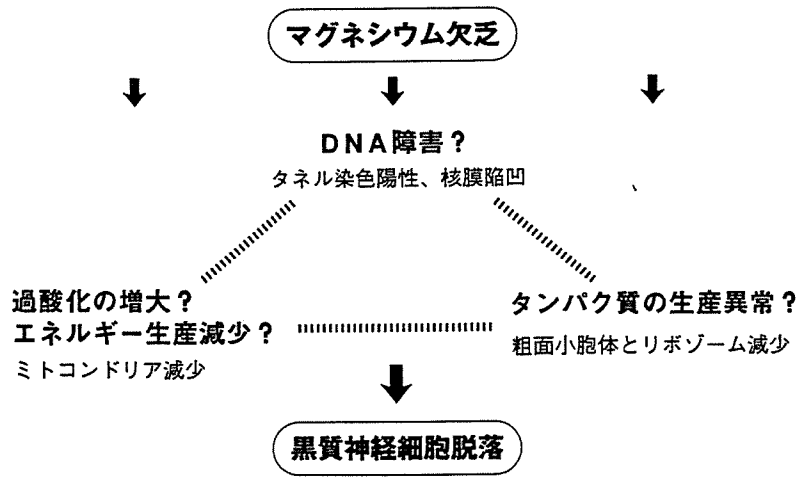

図5 世代にまたがるマグネシウム欠乏による黒質ドパミン神経細胞脱落の病的機構。

だけでは不変でも二世代目に異常が生じたのである。現代日本は壮大なミネラル欠乏状態に陥りつつあり、このままでは様々なミネラル欠乏症が子の世代に生じる可能性が危惧される。

マグネシウムを用いたパーキンソン病、パーキンソン痴呆症の予防と治療：本実験のデータを踏まえ、私どもはMgがパーキンソン病、パーキンソン痴呆症の新規治療法と成り得ないか、モデル実験系を使用した研究に着手した。現在のところ、培養黒質神経細胞を用いたパーキンソンモデル実験にMg投与が有意な効果を示す事を確認し(日本神経病理学会2005、2006、国際神経病理学会2006)、動物実験に入るところである。

References

1. Saris N-EL, et al. An update on physiological, clinical, and analytical aspects. *Clin Chim Acta* 294:1-26, 2000
2. Yase Y. The pathogenesis of amyotrophic lateral sclerosis. *Lancet* II: 292-296, 1972
3. Yase Y. ALS in the Kii peninsula: one possible etiological hypothesis. *In* Tsubaki T, Toyokura Y (eds): Amyotrophic lateral sclerosis, pp. 307-318, University of Tokyo Press, Tokyo, Japan, 1976
4. Gajusek DC, et al. Amyotrophic lateral sclerosis and parkinsonian syndromee in high incidence among the Auyu and Jakai people of west New Guinea. *Neurology* 32:107-126, 1982
5. Spencer PS, et al. Guam amyotrophic lateral sclerosis-parkinsonism dementia linked to a plant excite neurotoxin. *Science* 237:517-522, 1987
6. Yasui M, et al. Evaluation of Mg, Ca and Al metabolism in rats and monkeys maintained on Ca deficient diets. *Neurotoxicology* 12:603-614, 1991
7. Yasui M, et al. Effects of calcium-deficient diets in the central nervous system and bones of rats. *Neurotoxicology* 16:511-517, 1995
8. Yasui M, et al. Effects of low Ca and Mg dietary intake on the central nervous system of rats and calcium-magnesium related disorders in the amyotrophic lateral sclerosis focus in the Kii peninsula of Japan. *Magnes Res* 10:39-49, 1997
9. Oyanagi K, et al. Amyotrophic lateral sclerosis of Guam: the nature of the neuropathological findings. *Acta Neuropathol* 88:405-412, 1994

本研究は、東京都神経科学総合研究所河上江美子、菊池香会、緒方謙太郎、大原和彦、山形大学医学部第三内科　和田　学、和歌山県立医科大学神経内科　紀平為子、安井内科　安井昌之との共同研究であり、2002年米国神経病理学会ワイル賞(最優秀論文賞)受賞、2002年東京都知事表彰。
Oyanagi K, et al. Magnesium deficiency over generations in rats with special references to the pathogenesis of the parkinsonism-dementia complex and amyotrophic lateral sclerosis of Guam, Neuropathology, 26, 115-128, 2006 として発表。文月会(2004年1月24日)にて講演。

▶▶▶文　献◀◀◀
1) 田宮知耻夫：内科レントゲン診断学II，南山堂，東京，1939.
2) 福田　正：臨床放射線学，医学書院，東京，1968.
3) 多田信平，編著：X線解剖学図譜，マグプロス出版，東京，1979.
4) 田坂　皓，他編：放射線医学大系19B　胃II，中山書店，東京，1983.
5) 立入　弘，他編著：放射線医学入門，南山堂，東京，1970.
6) 坂井建雄，他編：人体の正常構造と機能III　消化管，日本医事新報社，東京，2000.

◆◆◆回　答◆◆◆

東京医科大学消化器内科客員教授
酒井義浩

ミネラルと神経変性疾患

Q カルシウムやマグネシウムは中枢神経組織や骨で重要な役割を持つ。ミネラルが関与すると推定されている中枢神経の変性疾患として、筋萎縮性側索硬化症やパーキンソニズム痴呆症が挙げられる。それらの多発地であるグアムや紀伊半島南部、西ニューギニアの環境分析で、河川、土壌中の低カルシウム、低マグネシウム、高アルミニウムが指摘され、このようなミネラル関連疾患の発生が増えることが予想されるというが、ミネラル関連疾患の概念、定義、病態、治療、予防のup to dateについて、文献を併せて。

（青森県　W）

A ミネラルとは、生体の生理的作用に必要な無機物のことである。カルシウム、リン、マグネシウム、ナトリウム、カリウム、鉄、銅、セレン、マンガン、亜鉛、コバルトなどが代表的なミネラルで、いわゆる必須微量金属も含まれる。

ミネラル関連疾患は、狭義にはこれらの摂取不足や過剰摂取が主たる原因である疾患をいう。遺伝的素因が主な原因で金属欠乏や沈着を起こす疾患、例えばヘモクロマトーシス（鉄沈着）やウィルソン病（銅沈着）などは広義のミネラル関連疾患とみなされる。また、パーキンソン病黒質の鉄沈着など、病変部にミネラル沈着が認められれば広義の関連疾患に含まれることがある。

ご質問はミネラルと、主として壮・老年期に発症する神経変性疾患との関連についてのものと考えられ、以下、それについて記載する。これに関連して「ミネラル」とみなされていない金属（アルミニウム）による中毒症にも触れる必要があるので、付け加える。

(1) ミネラルとの関連が指摘された神経変性疾患

①パーキンソン痴呆症（PDC）と筋萎縮性側索硬化症（ALS）

不思議なことに、この2疾患が東経140度線上の紀伊半島、グアム島、西ニューギニアに多発していた。グアム島での発症のピークは1950～60年頃といわれ、わずか30年ほどで急激に減少したことからも、主原因は外因とみなされている。これら三地域では土壌も飲料となる河川水も、低カルシウム、低マグネシウム、高アルミニウムであるという[1)2)]。

この所見に基づいた動物実験が多数行われた。筆者らは、ラットを用いた世代にまたがるマグネシウム長期欠乏がPDCに類似する黒質神経細胞脱落を引き起こすことを見出し[3)]、紀平らはマウスを用いた長期間低カルシウム、低マグネシウム、高アルミニウム摂取が大脳皮質神経細胞に、これもPDCに類似するリン酸化タウ蛋白の沈着を引き起こすことを報告した[4)]。すなわちPDCの黒質病変にはマグネシウム欠乏が、神経原線維変化（リン酸化タウが主成分）にはアルミニウム過剰摂取が関連している可能性がある。

②アルツハイマー病（AD）

動物脳内に直接アルミニウムを注入した際に神経細胞変性が生じ[5)]、AD脳内の神経原線維変化にアルミニウム沈着が報告され[6)]、ADはアルミニウム中毒症ではないか、と社会問題になった。しかし、飲料水などの疫学的調査では相反する所見が報告されており、未だ明確でない。

(2) ミネラル／金属関連疾患の成因

経口摂取による金属中毒症は、何らかの産業活動と関連していることが多い。日本で発生した有機水銀中毒、ヒ素中毒などである。一方、経口のミネラル欠乏は土地の風土や社会現象などとの関連が深い。上記したグアム島やニューギニアでは風土そのものであった。

ところが、文明が発達したと思われる現代の日本でも若い世代ほどミネラルの摂取量が少なく、マ

グネシウムなどは理想の摂取量の半分以下という。過度のダイエットや食生活の変化、特に食事代わりにお菓子を食することなどが原因といわれる[7][8]。

筆者らによる前記の実験では、マグネシウムを正常の5分の1まで減らしたラットの仔が、壮年までその餌を食べ続けた時、黒質変性を生じた。一世代だけでは不変でも二世代目に異常が生じたのである。現代日本人は壮大なミネラル欠乏状態に陥りつつあり、このままではさまざまなミネラル欠乏症が子の世代に生じる可能性が危惧される。

文献

1) Yase Y : Amyotrophic lateral sclerosis, Tsubaki T, et al ed, 1976, p307.
2) Gajdusek DC, et al : Neurology 32 : 107, 1982.
3) Oyanagi K, et al : Neuropathology 26 : 115, 2006.
4) Kihira T, et al : Neuropathology 22 : 171, 2002.
5) Klatzo I, et al : J Neuropathol Exp Neurol 24 : 187, 1965.
6) Perl DP, et al : Science 208 : 297, 1980.
7) 毎日新聞, 10月7日号, 1996.
8) アエラ, 9月2日号, 2002, p49.

精神神経科

双極性障害の治療

Q 双極性障害（bipolar disease：BP）へのアリピプラゾールやガバペンチンの使用法を具体的に。

（大阪府　Y）

A 難治性うつ病患者の病歴を子細に検討すると軽躁病相の存在が認められることが多く、予想外に双極性障害（BP）が多いことが近年、次第に明らかになってきた。気分安定薬としてリチウム、バルプロ酸、カルバマゼピンが用いられているが、臨床効果の点で必ずしも満足できるものではない。新規抗精神病薬や新しい抗てんかん薬がBPに試みられている。

最近日本で認可された新規抗精神病薬アリピプラゾール、抗てんかん薬ガバペンチンのBPに対する使用法についてのご質問であるが、まず、これらの薬物のBPに対する有効性を紹介した後に、使用法の注意を述べる。

◆◆◆回　答◆◆◆

東京都神経科学総合研究所運動・感覚システム研究分野長・神経病理学

小柳清光

アリピプラゾールは、BPⅠ型の躁病あるいは混合性エピソードの急性期に対してプラセボより有効なこと、26週間ではあるが躁病や混合性エピソードの再発防止効果がプラセボより優れていることが二重盲検試験で認められている。またアリピプラゾール15～30mg／日とハロペリドール10～15mg／日は、多施設共同二重盲検試験において同等の効果を示した[1]。米国においてアリピプラゾールは、2002年に統合失調症に、2004年にBPの急性期躁病に、そして2005年にBPの再発防止に認可された。日本では、2006年に統合失調症に対して認可された。しかし、BPには認可されていない。

アリピプラゾールはD_2受容体部分アゴニストであり、その特徴は、ドパミン活動の亢進時にはアンタゴニストとして固有活性のレベルまで抑制し、低下時にはアゴニストとして固有活性のレベルまで回復させることにある。この特徴を最大限に引き出すには、単剤使用が望ましい[1]。しかし、BPの治療では気分安定薬や抗うつ薬などの併用が行われる可能性が高い。本剤の実際の臨床での使用は統合失調症において始まったばかりであり、これから具体的な活用の工夫が始まるところである。

ガバペンチンは、抑制神経であるGABA神経系の機能を維持・増強する抗てんかん薬である。BPに対する20のオープン試験の結果をまとめた報告[2]では、患者全体では66％（225／339人）に、躁病、軽躁病、混合状態では76％（62／82人）に、そしてうつ病では55％（46／83人）に改善がみられている。予防効果については、改善が維持されたのは18人中7人だけであった。リチウム、バルプロ酸あるいは両者の併用を2週間続けたが改善不十分な急性の躁病患者に対するガバペンチン900～3600mg／日と、プラセボの無作為化二重盲検試験では、プラセボ群のほうが症状改善効果が優れていた[3]。

ガバペンチンは就寝前に300mg／日から開始し、必要に応じて

J Hum Genet (2006) 51:341–352
DOI 10.1007/s10038-006-0369-6

ORIGINAL ARTICLE

Hitoshi Sakuraba · Yasunori Chiba · Masaharu Kotani
Ikuo Kawashima · Mai Ohsawa · Youichi Tajima
Yuki Takaoka · Yoshifumi Jigami · Hiroshi Takahashi
Yukihiko Hirai · Takashi Shimada
Yasuhiro Hashimoto · Kumiko Ishii
Toshihide Kobayashi · Kazuhiko Watabe
Tomoko Fukushige · Tamotsu Kanzaki

Corrective effect on Fabry mice of yeast recombinant human α-galactosidase with *N*-linked sugar chains suitable for lysosomal delivery

Received: 20 November 2005 / Accepted: 20 December 2005 / Published online: 11 March 2006

Abstract We have previously reported the production of a recombinant α-galactosidase with engineered *N*-linked sugar chains facilitating uptake and transport to lysosomes in a *Saccharomyces cerevisiae* mutant. In this study, we improved the purification procedure, allowing us to obtain a large amount of highly purified enzyme protein with mannose-6-phosphate residues at the non-reducing ends of sugar chains. The products were incorporated into cultured fibroblasts derived from a patient with Fabry disease via mannose-6-phosphate receptors. The ceramide trihexoside (CTH) accumulated in lysosomes was cleaved dose-dependently, and the disappearance of deposited CTH was maintained for at least 7 days after administration. We next examined the effect of the recombinant α-galactosidase on Fabry mice. Repeated intravascular administration of the enzyme led to successful degradation of CTH accumulated in the liver, kidneys, heart, and spleen. However, cleavage of the accumulated CTH in the dorsal root ganglia was insufficient. As the culture of yeast cells is easy and economical, and does not require fetal calf serum, the recombinant α-galactosidase produced in yeast cells is highly promising as an enzyme source for enzyme replacement therapy in Fabry disease.

Keywords Fabry disease · α-Galactosidase · Ceramide trihexoside · Yeast · Enzyme replacement therapy · Fabry mouse

Introduction

Lysosomal α-galactosidase (EC 3.2.1.22) is a critical enzyme for the cleavage of glycolipids with terminal α-D-galactosyl residues, primarily ceramide trihexoside (CTH; also called globotriaosylceramide, GL-3, and

H. Sakuraba (✉) · M. Kotani · I. Kawashima · M. Ohsawa
Y. Tajima
Department of Clinical Genetics,
The Tokyo Metropolitan Institute of Medical Science,
Tokyo Metropolitan Organization for Medical Research,
3-18-22 Honkomagome,
Bunkyo-ku, Tokyo 113-8613,
Japan
E-mail: sakuraba@rinshoken.or.jp
Tel.: +81-3-38232105
Fax: +81-3-38236008

Y. Chiba · Y. Takaoka · Y. Jigami
Research Center for Glycoscience,
National Institute of Advanced Industrial Science and Technology,
1-1-1 Higashi, Tsukuba 305-0044, Japan

M. Ohsawa
CREST, JST, 4-1-8 Hon-machi,
Kawaguchi 332-0012, Japan

H. Takahashi · Y. Hirai · T. Shimada
Department of Biochemistry and Molecular Biology,
Nippon Medical School, 1-1-5 Sendagi, Bunkyo-ku,
Tokyo 113-8602, Japan

Y. Hashimoto · K. Ishii · T. Kobayashi
Supra-Biomolecular System Research Group,
RIKEN Frontier Research System, 2-1 Hirosawa,
Wako 351-0198, Japan

K. Watabe
Department of Molecular Neuropathology,
Tokyo Metropolitan Institute for Neuroscience,
Tokyo Metropolitan Organization for Medical Research,
2-6 Musashidai, Fuchu 183-8526, Japan

T. Fukushige · T. Kanzaki
Department of Dermatology,
Kagoshima University Graduate School of Medical and Dental Sciences, 8-35-1 Sakuragaoka, Kagoshima 890-8520, Japan

Gb_3) in lysosomes. Lysosomal α-galactosidase is a glycoprotein, and is synthesized in rough-surfaced endoplasmic reticulum followed by the addition of *N*-linked high-mannose-type oligosaccharides. The enzyme is then transferred to the Golgi apparatus, where further modification, including addition of mannose-6-phosphate (M6P) residues and binding to M6P receptor, occurs. Subsequently, the enzyme is transported to endosomes via M6P receptors. The enzyme then moves to lysosomes, where it exerts its function. In some type of cells, including cultured fibroblasts, α-galactosidase can be incorporated into the cells from the extracellular milieu via M6P receptors on the plasma membrane and transported to lysosomes (Kornfeld and Sly 2001).

A deficiency of α-galactosidase results in widespread cellular deposition of CTH, thereby causing Fabry disease (MIM 301500) (Desnick et al. 2001). Fabry disease is an X-linked genetic disease exhibiting a wide clinical spectrum. Male patients with classic Fabry disease usually have no α-galactosidase activity and, in childhood or adolescence, there is pain in the peripheral extremities, angiokeratoma, hypohidosis and corneal opacity, followed by renal, cardiac and cerebrovascular involvement with increasing age (Desnick et al. 2003). The incidence of classic Fabry disease has been estimated to be 1 in 40,000 male newborns (Desnick et al. 2001). Patients with variant form Fabry disease have residual α-galactosidase activity and milder clinical manifestations with late onset (Sakuraba et al. 1990; Nakao et al. 1995). Females heterozygous for Fabry disease can be affected to a moderate or severe degree due to random X-chromosomal inactivation (Sakuraba et al. 1986; Fukushima et al. 1995; Itoh et al. 1993, 1996; Lyon 1962). However, a recent survey has revealed that many Fabry females can be affected similarly to Fabry males and thus should be considered as patients rather than carriers of the disease (Mehta et al. 2004). Fabry disease has been under-recognized, and the number of Fabry patients requiring treatment is thought to be much larger than previously assumed.

Recently, two different recombinant α-galactosidases were developed for enzyme replacement therapy for Fabry disease: agalsidase alfa (Replagal; Transkaryotic Therapies, Cambridge, MA) generated in human cultured fibroblasts (Schiffmann et al. 2000), and agalsidase beta (Fabrazyme; Genzyme Therapeutics, Cambridge, MA) produced in Chinese hamster ovary (CHO) cells (Eng et al. 2001a, b). The former has been approved in Europe, and the latter in Europe, the United States, and Japan, and many Fabry disease patients have been successfully treated with these drugs. However, these recombinant enzymes are produced in cultured mammalian cells and thus their production is very expensive. Furthermore, careful monitoring for infection by pathogens is essential because fetal calf serum is usually required for the culture of mammalian cells.

We have constructed a yeast cell line producing a recombinant human α-galactosidase with *N*-linked high-mannose-type sugar chains (yeast recombinant human α-galactosidase, yr-haGal), as described previously (Chiba et al. 2002). Effective incorporation of the enzyme into affected organs is very important for enzyme replacement therapy, and in Fabry disease successful targeting of α-galactosidase is strongly dependent on the presence of M6P residues on the sugar chains of the enzyme preparations. In this study, we improved the procedures for purification of α-galactosidase from the culture medium of yeast cells to obtain a large amount of highly purified enzyme protein with M6P residues that facilitate incorporation of the enzyme into affected organs, and analyzed the effect of the purified enzyme on cleavage of CTH accumulated in cultured Fabry fibroblasts and organs of Fabry mice.

Materials and methods

Purification of yr-haGal secreted into the culture medium of yeast cells

Here we used a yeast strain, HPY21G, constructed by introducing the human α-galactosidase cDNA into a *Saccharomyces cerevisiae* strain, HPY21, as described previously (Chiba et al. 2002). A large-scale culture (100 l) was performed to examine the effect of yr-haGal on Fabry mice. We had previously used Blue-Sepharose and ConA-Sepharose columns to purify yr-haGal (Chiba et al. 2002). However, these columns are very expensive and had only weak binding ability because of the characteristics of the affinity chromatography so we improved the purification procedure. All column materials used in the experiments reported here were purchased from Amersham Biosciences Japan (Tokyo, Japan). The culture medium of the HPY21G strain was collected and concentrated, and ammonium sulfate was added slowly to the supernatant to a final concentration of 55%. The precipitate was recovered by centrifugation, re-dissolved in 25 mM 2-(*N*-morpholino)ethanesulfonic acid (MES) buffer, pH 6.0, and then dialyzed against the same buffer. A sample was then applied to a HiLoad Q 16/10 Sepharose HP column equilibrated with the same buffer. After washing the column, α-galactosidase was eluted with a 0–1 M NaCl gradient in the same buffer. Fractions containing enzyme activity were pooled, and then a one-tenth volume of 3 M ammonium sulfate was added. A sample was then applied to a HiLoad 26/10 Phenyl HP column equilibrated with 25 mM MES buffer, pH 6.0, containing 0.3 M ammonium sulfate. After washing the column, α-galactosidase was eluted with a 0.3–0 M ammonium sulfate gradient in the same buffer. Fractions containing enzyme activity were dialyzed against 20 mM Tris–HCl buffer, pH 7.5, containing 150 mM NaCl, and then were concentrated with an Amicon Ultra-4 (13,000 MWCO; Millipore, Bedford, MA). A sample was then applied to a HiLoad 16/60 Superdex 200pg column. Fractions containing enzyme activity then were pooled and subjected to α-mannosidase treatment to expose M6P residues at

the non-reducing ends of the sugar chains. Treatment of the recombinant α-galactosidase with the culture supernatant of SO-5, a new bacterium producing an α-mannosidase, was performed as described previously (Chiba et al. 2002). After the α-mannosidase treatment, the α-galactosidase protein was re-purified on HiLoad Q and HiLoad 16/60 Superdex 200pg columns under the conditions described above.

Biochemical analyses of the enzymatic properties of yr-haGal

The purity and molecular mass of yr-haGal produced in yeast cells were determined by sodium dodecyl sulphate polyacrylamide gel electrophoresis (SDS-PAGE) as described previously (Chiba et al. 2002). Reversed-phase high-performance liquid chromatography (HPLC) analysis of the purified yr-haGal was performed on a Cosmosyl $5C_4$-AR-300 (4.6×150 mm) column (Nacalai Tesque, Kyoto, Japan). The protein was eluted with a linear trifluoroacetic acid/acetonitrile gradient at a flow rate of 1 ml/min with ultraviolet detection at 215 nm. Deglycosylation of yr-haGal with *N*-glycanase F (Takara Bio, Shiga, Japan) was performed according to the method recommended by the manufacturer, and *N*-terminal amino acid sequence analysis and matrix-assisted laser desorption ionization time-of-flight mass spectrometry (MALDI-TOF-MS) analysis were performed by Shimazu Corporation (Kyoto, Japan).

α-Galactosidase activity was measured fluorometrically with 4-methylumbelliferyl-α-galactopyranoside (Calbiochem, San Diego, CA) as a substrate in the presence of *N*-acetylgalactosamine (Sigma, St. Louis, MO), a specific inhibitor of α-*N*-acetylgalactosaminidase (Mayes et al. 1981). The protein concentration was determined with a *DC* assay kit (Bio-Rad, Richmond, CA), using bovine serum albumin (BSA) as a standard.

Sugar chain analysis of yr-haGal was performed according to the method reported previously (Takashiba et al. 2004). Briefly, the enzyme was hydrolyzed with 2 M trifluoroacetic acid and L-rhamnose, as an internal standard, at 100°C for 2 h, and monosaccharides derived from the sugar chains were then quantitated by means of capillary electrophoresis using a P/ACE MDQ equipped with a laser-induced fluorescence detector (Beckman Coulter, Fullerton, CA); authentic monosaccharides were used as standards for quantitation.

Examination of the effect of yr-haGal on cultured human Fabry fibroblasts

Cultured fibroblasts from a patient with Fabry disease and a normal control subject were established and maintained in our laboratory. The cells were cultured in Ham's F-10 medium containing 10% fetal calf serum and antibiotics at 37°C in an incubator containing 5% CO_2. The study involving the cultured human fibroblasts was approved by the Ethical Committee of our institute.

To examine uptake of yr-haGal by Fabry fibroblasts, yr-haGal produced in yeast cells was added to the culture medium of Fabry fibroblasts to give concentrations of 0, 0.25, 0.5, 1.0, 3.0 and 6.0 μg/ml. For examination of the inhibitory effect of M6P on the cellular uptake of yr-haGal, Fabry fibroblasts were cultured in medium containing 5 mM M6P and 1.0μg/ml yr-haGal. After 18 h culture, the cells were harvested mechanically, washed three times with phosphate-buffered saline (PBS), pH 7.4, and then collected as a pellet by centrifugation. An appropriate amount of water was then added to the pellet and the cells were sonicated; the resulting homogenate was used for α-galactosidase assay and protein determination.

To examine degradation of accumulated CTH by the incorporated recombinant α-galactosidase, Fabry fibroblasts were cultured with culture medium containing the recombinant α-galactosidase at concentrations of 0, 0.5, 1.0, 2.0 and 3.0μg/ml for 3 days. Alternatively, Fabry fibroblasts were cultured in medium containing 3.0μg/ml recombinant α-galactosidase for 0, 1, 3, 5, and 7 days. Cells grown on a Lab-Tek chamber slide (Nunc, Naperville, IL) were fixed with 2% paraformaldehyde in PBS, pH 7.4, for 10 min, followed by blocking with 5% BSA in PBS for 1 h. The cells were then incubated with a mouse monoclonal anti-CTH antibody (culture supernatant; IgG isotype) (Kotani et al. 1994) and rabbit polyclonal anti-α-galactosidase antibodies (1:100 diluted; IgG isotype) (Ishii et al. 1994) for 1 h. After washing, they were reacted for 1 h with a fluorescent isothiocyanate-conjugated goat anti-mouse IgG $F(ab')_2$ (diluted 1:200; Jackson Immuno Research, West Grove, PA) and a rhodamine-conjugated goat anti-rabbit IgG $F(ab')_2$ (diluted 1:400; Jackson Immuno Research). To determine the localization of the accumulated CTH, double staining with the anti-CTH antibody and a mouse monoclonal antibody to lysosome-associated membrane protein-1 (LAMP-1; Southern Biotechnology, Birmingham, AL), a marker for lysosome, was also performed according to a modified method described elsewhere (Kotani et al. 2004). The stained cells were observed under a microscope (Axiovert 100M; Zeiss, Oberkochen, Germany) equipped with a confocal laser scanning imaging system (LSM510; Zeiss).

Examination of the effect of yr-haGal on Fabry mice

Fabry mice (α-galactosidase knock-out mice, donated by Ashok B. Kulkarini and Toshio Oshima) and wild type C57BL/6 mice were used in this experiment according to the rules drawn up by the Animal Care Committee of our institute.

To examine the pharmacokinetics and biodistribution of the recombinant α-galactosidase, a single dose, 3.0 mg/kg body weight, of recombinant α-galactosidase was injected into the tail veins of Fabry mice. As a control, a single dose, 2.0 mg/kg body weight of agalsidase beta (purchased from Genzyme Japan, Tokyo, Japan)

was injected into litter-matched Fabry mice so that the injected enzyme activity was almost the same (6.0–6.4 mmol h^{-1} kg^{-1} body weight). Each group consisted of two mice. Blood samples were collected at 0, 1, 3, 5, 10, 20, 30, and 40 min after injection of the enzymes, and a time course of changes in α-galactosidase activity in plasma was determined. The mice were sacrificed at 1 h after administration of the enzymes, and their livers, kidneys, hearts, and spleens were then removed. Tissue samples were then homogenized in citrate-phosphate buffer, pH 4.6, and centrifuged. The resulting supernatants were assayed for α-galactosidase activity.

To examine cleavage of the CTH accumulated in organs, two groups of litter-matched Fabry mice, each consisting of three mice, were repeatedly injected with the recombinant α-galactosidase, 3.0 mg/kg body weight, and agalsidase beta, 2.0 mg/kg body weight, separately every week for four doses, and then sacrificed 6 days after the last injection. Their livers, kidneys, hearts, spleens, and dorsal root ganglia were then removed, and used as samples for biochemical and/or morphological analyses.

For immunohistochemical analysis, the mouse tissues were stored at −80°C before use, and then frozen sections of 10μm thickness were fixed with 4% paraformaldehyde in PBS for 5 min at room temperature. The specimens were incubated with PBS containing 5% (w/v) BSA for 30 min at room temperature to block nonspecific binding. Subsequently, the samples were treated with a mouse monoclonal anti-CTH antibody (culture supernatant; IgG isotype) for 1 h at room temperature, and then treated with fluorescent isothiocyanate conjugated goat anti-mouse IgG $F(ab')_2$ (diluted 1:200; Jackson Immuno Research). The stained tissues were examined under a confocal laser scanning microscope as described above.

For determination of CTH levels, tissues, including liver, kidney, heart, and spleen, were analyzed by means of thin-layer chromatography, followed by densitometry according to the method described previously (Takahashi et al. 2002).

For morphological examination, kidney tissues were cut into small pieces, and then fixed in cold 2.5% glutaraldehyde and 2% paraformaldehyde in 0.1 M phosphate buffer, pH 7.4. The specimens were rinsed in PBS, and then postfixed with 2% osmium tetraoxide in 0.2 M sucrose in PBS for 1 h and dehydrated with graded concentrations of ethanol, 50% through absolute, and glycidyl *n*-butyl ether. Dehydrated specimens were then embedded in Epon 812 resin. Sections of 0.1μm thickness were prepared and stained with 2% uranyl acetate in 50% ethanol for 5 min, restained with Reynolds lead citrate for 3 min, and finally examined under an electron microscope (Hitachi H-7100; Hitachi, Tokyo, Japan).

Examination of the anti-α-galactosidase immune reaction

To determine whether or not Fabry mice injected with the enzymes produced antibodies against the enzymes, solid-phase enzyme-linked immunosorbent assay (ELISA) was performed. Serum samples were obtained from Fabry mice repeatedly injected with yr-haGal (3.0 mg/kg body weight), and agalsidase beta (2.0 mg/kg body weight) separately every week for four doses. Briefly, a 96-well flat bottom microplate for ELISA (Immulon 2 HB; Thermo Lab Systems, Flanklin, MA) was coated with 1.0 μg/ml of the enzymes in PBS. After washing 5 times with 1% BSA in PBS, 200 μl 1% BSA in PBS was added to each well as a blocking solution, followed by incubation for 1 h at room temperature. After removing the blocking solution, 100 μl of the mouse sera or rabbit anti-α-galactosidase antibodies (Ishii et al. 1994) diluted to various concentrations was added to each well, followed by incubation for 1 h. The wells were then washed, incubated in 100 μl peroxidase-conjugated anti-mouse IgG $F(ab')_2$ (diluted 1: 2,000; Jackson Immuno Research) for 45 min, washed again, and finally incubated in 100 μl *O*-phenylenediamine (Sigma) generated as 0.4 mg/ml 0.05 M citrate-phosphate buffer, pH 5.0. After incubation with the chromogenic substrate for 10 min, the optical density of each well was measured by means of an ELISA reader (Bio-Rad, Hercules, CA).

Results

Properties of yr-haGal

The new purification method described in this paper allowed us to treat a large volume of culture medium and obtain highly purified yr-haGal with 870-fold purifica-

Table 1 Monosaccharide analysis. *M6P* Mannose-6-phosphate, *yr-haGal* yeast recombinant human α-galactosidase

	yr-haGal[a] (mol/mol protein)	Agalsidase beta[b] (mol/mol protein)	Agalsidase alfa[b] (mol/mol protein)
M6P	3.8±0.2	3.1±0.1	1.8±0.0
Galactose	ND[c]	8.0±0.4	12.2±1.0
Fucose	ND	1.8±0.1	3.0±0.3
N-Acetylglucosamine	0.8±0.6	18.4±0.4	22.5±2.3
Mannose	53.8±2.6	25.7±1.8	27.6±0.5
Sialic acid	ND	7.0±1.0	6.9±0.6

[a]Values expressed as means ±SD, $n=3$
[b]Lee et al. 2003
[c]Not detected